Available online at www.sciencedirect.com
ScienceDirect
Magnetic Resonance Imaging 25 (2007) 923–932
MAGNETIC RESONANCE IMAGING

Evaluating gradient artifact correction of EEG data acquired simultaneously with fMRI

Petra Ritter*, Robert Becker, Christine Graefe, Arno Villringer

Berlin NeuroImaging Center and Charité, Universitätsmedizin Berlin, Berlin, Germany

Accepted 11 January 2007

Abstract

Simultaneous electroencephalography (EEG) and functional magnetic resonance imaging (fMRI) has become a widely used application in spite of EEG perturbations due to electromagnetic interference in the MR environment. The most prominent and disturbing artifacts in the EEG are caused by the alternating magnetic fields (gradients) of the MR scanner. Different methods for gradient artifact correction have been developed. Here we propose an approach for the systematic evaluation and comparison of these gradient artifact correction methods. Exemplarily, we evaluate different algorithms all based on artifact template subtraction — the currently most established means of gradient artifact removal. We introduce indices for the degree of gradient artifact reduction and physiological signal preservation. The combination of both indices was used as a measure for the overall performance of gradient artifact removal and was shown to be useful in identifying problems during artifact removal. We demonstrate that the evaluation as proposed here allows to reveal frequency-band specific performance differences among the algorithms. This emphasizes the importance of carefully selecting the artifact correction method appropriate for the respective case.

Keywords: Simultaneous EEG-fMRI; Gradient artifact correction; Functional MRI

1. Introduction

Simultaneous electroencephalography (EEG) and functional magnetic resonance imaging (fMRI) has become a widely used application for bimodal noninvasive imaging of human brain function [1]. By the combination of the two methods their complementary features — good spatial resolution of fMRI and high temporal resolution and assessment of direct neural activity of EEG — can be utilized. This has found application in a multitude of studies and has proven to be useful for the investigation of fMRI correlates of spontaneous EEG rhythms [2–7], event-related brain responses [8–10], sleep stages [11,12] and epileptic activity [13–20]. However, even with an optimized EEG–fMRI setup EEG data collected in such experiments contain artifacts caused by static and changing magnetic fields of the MR scanner. Two types of scanner environment artifacts can be distinguished: (I) Pulsatile blood movement causes body and electrode movements inside the static magnetic field (B_0) of the scanner which generates the so-called ballistocardiogram with amplitudes on the order of brain electrical signals [21–23]. (II) During MR image acquisition, switching of magnetic field gradients produces artifacts in the EEG data. The amplitude of these gradient artifacts can be more than two orders of magnitude higher than the physiological EEG signal.

Methods to remove the ballistocardiogram include, for example, subtraction of its electrocardiogram (ECG) time-locked average waveform [21], subtraction of an amplitude adapted dynamic template calculated by sliding average [9] or by independent component analysis [24]. Similarly, for the correction of gradient artifacts that are in the focus of this study, different methods have been proposed. One is the comparison of the spectral content of EEG data acquired with simultaneous MR acquisition and that of EEG data without MR acquisition. Subsequently, MR-specific frequencies are filtered out [25]. The disadvantage of this method is that due to a spectral overlap between the physiological EEG (in the following referred to as 'biosignal') and gradient artifacts, a part of the biosignal is

* Corresponding author. Berlin NeuroImaging Center, Department of Neurology, Charité-Universitätsmedizin Berlin, 10117 Berlin, Germany. Tel.: +49 30 450560005; fax: +49 30 450560952.
E-mail address: petra.ritter@charite.de (P. Ritter).

0730-725X/$ – see front matter © 2007 Elsevier Inc. All rights reserved.
doi:10.1016/j.mri.2007.03.005

removed from the EEG [13]. In addition, this approach may suffer from the ringing effect of frequency domain filters [13]. A similar approach relies on subtraction of an average gradient artifact spectrum from the spectrum of the artifact distorted EEG in the frequency domain [26]. Another more widely used method known as 'artifact-template subtraction' has been proposed by Allen et al. [27]. This approach assumes that the shape of gradient artifacts is constant over time and additive to the physiological signal. It acknowledges the fact of considerable spectral overlapping of artifacts and physiological EEG data. The artifact template computed by averaging several artifact epochs is subsequently subtracted from the artifact-afflicted EEG. This type of correction algorithm has been successfully adopted for the reconstruction of spontaneous EEG signatures such as alpha rhythm [4,6,7] and epileptic activity [13,18,28]. It has been validated by demonstrating that visual evoked potentials acquired during and in between artifact periods showed high concordance after artifact correction [29]. Several algorithms for gradient artifact correction are based on template subtraction; however, they vary in some details. Up to now, no systematic approach for the evaluation and comparison of these algorithms has been proposed. Usually, a single algorithm is employed within an EEG–fMRI study and often the quality of gradient artifact correction is assessed by visual inspection only. The choice of the correction algorithms sometimes seems to be rather arbitrary. At first sight, the employed approach seemingly delivers sufficient results after filtering and averaging procedures. However, particularly for the analysis of unaveraged EEG data, when residual artifacts are not averaged out and for the analysis of specific spectral bands, a differentiated knowledge of the strengths and weaknesses of the available gradient correction algorithms is essential. Different approaches for quality assessment of artifact removal exist. For example, by means of a phantom and an artificially generated voltage signal the degree of reconstruction of the original signal after artifact correction can be assessed [30]. The time course of the phantom signal before artifact induction is precisely known, which is not the case for the original EEG during MR acquisition. Thus, a phantom measurement seems to be the most elegant evaluation approach. The disadvantages, however, are (I) the need for the technical setup of a phantom measurement; (II) assessment of an artificial signal not necessarily reflecting the complexity of a physiological signal; (III) unnatural experimental conditions, for example no subject movements; and (IV) generalizing on the performance of the algorithm without considering variability of artifact removal in individual natural EEG data sets.

The alternative to phantom measurements is using real EEG data for the evaluation of gradient artifact correction. For example, the EEG trace recorded within the MR scanner without MR acquisition can be compared to the EEG trace recorded simultaneously with fMRI, for example, in terms of its spectral content [27]. A major drawback of this approach is the lack of knowledge of the original EEG signal obscured by the gradient artifact. For example, the serial acquisition of one epoch of gradient artifact-free EEG and one epoch of gradient artifact-afflicted EEG bears the risk of systematic effects as for instance drifts of vigilance, attention, etc. In order to reduce such effects, we propose simultaneous EEG–fMRI acquisition with fast alternating and evenly distributed nonacquisition and acquisition epochs. Since this design is already quite common for fMRI studies, individual data sets of such studies could directly be evaluated in respect to artifact removal quality without the need for additional data. Based on this idea, the aim of this article was to demonstrate how the performance of gradient correction algorithms can be evaluated in such typical data sets. To this end, we selected different gradient artifact correction algorithms based on the approach of template artifact subtraction. The performance is assessed in terms of quality of artifact removal; neither computational efficiency nor stability of the programs is evaluated in this work.

It is important to note that two different types of technical setups are possible for simultaneous EEG–fMRI acquisition. The so far most established setup runs EEG and fMRI acquisition independently of each other. Since the gradient artifact contains high-frequency parts not fully covered with an EEG sample rate of 5 kHz, minimal deviations of the internal timing of each device cause a variable sampling of the gradient artifact in the EEG. This poses a particular challenge to artifact template subtraction-based correction algorithms. Alternatively, another more recently proposed approach is to synchronize the clocks of the EEG and the MR device [31]. Then, given the MR-scan repetition time is an integer multiple of the EEG sampling interval, gradient artifacts are constant over time and can be removed by simple artifact template subtraction [32]. Since synchronization of EEG and MR scanner requires technical modifications that are as yet available in only a few laboratories, the unsynchronized acquisition of EEG and fMRI is still the prevalent method. Therefore, in this study we focus on the more challenging gradient artifact removal of EEG data that have been acquired without EEG–fMRI synchronization.

To this end, EEG data sets acquired simultaneously with fMRI of subjects being exposed to visual checkerboard stimulation [29] were analyzed. A combination of the following analyses was employed for performance estimation: (I) The degree of artifact reduction was evaluated by comparing the spectral content of the corrected data to that of gradient-artifact free EEG epochs for six predefined frequency bands, ranging from theta to omega (1–250 Hz). (II) The preservation of non-gradient artifact components of the EEG after correction was evaluated twofold: by comparing the spectral content of nonacquisition EEG epochs before and after gradient artifact correction for the six predefined frequency bands and by exploring the impact of artifact correction on artificially generated signals added to the EEG.

2. Methods

All MR gradient-artifact[1] algorithms undergoing evaluation in this study incorporate an approach proposed by Allen et al. [27], but differing in some features. One algorithm is an in-house-developed MATLAB (V7.0.4, MathWorks, Natick, MA, USA) based script referred to as interpolation–template–alignment–subtraction (ITAS) that relies on interpolation of the data and alignment of the artifacts before artifact-template estimation and subtraction, closely following the suggestions by Allen et al. [27]. Further, two versions of the MR gradient removal tool contained in the Vision Analyzer software (versions V.1.05.0002 and V.1.05.0004, BrainProducts, Munich, Germany) are analyzed, which in contrast to ITAS do not perform data interpolation. The two remaining algorithms are versions of the MATLAB-based plug-in FMRI Artifact Slice Template Removal (FASTR, Center for Functional MRI of the Brain, Oxford, UK) of the open source toolbox EEGLab [33]. They are part of the FMRIB toolbox (V1.2b and V1.21) and, in addition to the approach of Allen et al. [27], offer a feature for removal of residual artifacts based on an optimal basis set (OBS) using principal component analysis (PCA) [34].

Since a criterion for the quality of artifact correction is biosignal preservation, in this study we attempt to avoid nonspecific broadband digital filtering offered by most of the algorithms.

2.1. Description of the algorithms tested

The in-house-built ITAS algorithm is a MATLAB-based script closely following the suggestions by Allen et al. [27]. In the following, we describe the operations the algorithm performs:

1. The data are divided into k epochs, each consisting of a MRI scan period and the subsequent interscan period. These epochs are baseline corrected using a customizable time window before scan start.
2. To account for temporal shifts between artifact periods, the data are interpolated with a customizable factor and subsequently aligned by maximizing cross-correlation to a reference period. After adjusting, epochs are down-sampled to the original sampling frequency.
3. For each epoch, an artifact template B_n (Eq. (1)) is calculated and subtracted (Eq. (2)). The template consists of a weighted average of n artifact epochs with stronger weights for adjacent artifacts to account for possible changes of the artifact waveform over time:

$$B_n = \frac{\sum_{i=1}^{k} w^{|n-i|} A_i}{\sum_{i=1}^{k} w^{|n-i|}} \quad (1)$$

$$C_n = A_n - B_n \quad (2)$$

where n is the epoch index, k the number of epochs (here $k=120$), w the weighting factor ($w=0.9$), A the individual epoch, B the artifact template, C the corrected epoch.

The Vision Analyzer algorithm (V.1.05.0002) for gradient artifact correction offers three different methods for template estimation. No interpolation and subsequent alignment of the data are performed. For template building, either (I) all epochs, (II) a sliding average of a certain number of epochs or (III) a predefined number of initial scan epochs plus the subsequent epochs exceeding a pre-defined cross-correlation with the initial template can be used.

In the most recent version of the Vision Analyzer (V.1.05.0004), template drift detection (TDD) and subsequent template drift correction are additionally offered. TDD finds temporal shifts between the average artifact template and the individual artifact. It adjusts the 'scan start' marker such that the drift is smaller than one sampling interval. With the use of the drift information provided by TDD, a customizable number of different average-artifact templates are calculated. Each individual artifact is assigned to one template. Artifact correction is obtained by subtraction of the corresponding template.

The EEGLab plug-in FMRIB with the gradient correction algorithm FASTR is freely available at http://www.fmrib.ox.ac.uk [34]. Version V.1.2 contains the following features:

The signal is interpolated, and subsequent adjustment and alignment of the artifact epochs are performed. For baseline correction, a 1-Hz high-pass filter merely for template estimation is applied, preserving original data. The number of the adjacent artifact epochs to be averaged can be selected. Residual artifacts are removed by fitting an OBS to the data. The OBS describes the temporal variation in the artifact and is based on temporal PCA. To avoid the effects of digital filtering, ANC is not used here. During the preparations for this manuscript, an updated version of FASTR has been released. One of the major changes as announced on the website was preventing overfitting of residuals caused by OBS. This version (FASTR 1.21) has also been evaluated in this study.

2.2. EEG data

We explored five EEG data sets simultaneously acquired with fMRI (1.5 T Vision MR tomograph, Siemens, Erlangen, Germany) taken from a previously published study [29]. Five healthy subjects (female: mean age 26.75 years; S.D. 2.50 years; range 23–30 years) with normal or corrected to normal vision underwent visual stimulation

[1] Since this study deals exclusively with gradient-artifact correction, we use the term 'artifact' throughout the paper when referring to gradient artifacts.

with a black-and-white circular reversing checkerboard during simultaneous EEG–fMRI acquisition. Written informed consent was obtained according to the Declaration of Helsinki. Please see Ref. [29] for stimulus and setup details. In short, subjects were asked to fixate the fixation cross of the stimulus and to avoid any movements or excessive eye blinks during the whole experiment. The visual stimulus was applied via a mirror above the subjects' heads, reflecting the image from a screen attached to the head coil. The stimulus was projected onto the acrylic screen through a collimating lens by a conventional video projector. Contrast reversal occurred once during an acquisition period and once during the nonacquisition period, each lasting 2.1 s. For each subject, 120 MR scans were recorded, comprising 120 trials within the artifact period and 120 trials within the nonartifact period. Data were recorded by an MR-compatible 32-channel EEG system (BrainAmp, Brain Products, Munich, Germany) with a sampling frequency of 5 kHz, an analogous 250-Hz low-pass filter and 0.1-Hz high-pass filter. No digital filters were applied. For evaluation of the algorithms, we analyzed occipital channel O2 according to the 10-20 International System. Functional imaging was performed by a 1.5 Tesla whole body MR scanner (Magnetom Vision; Siemens, Erlangen, Germany) using a T2*-weighted BOLD-sensitive gradient echo planar imaging sequence [35–38]. The fMRI parameters were as follows: TE 60 ms, flip angle 90°, matrix 64×64, voxel size 3.3×3.3×5 mm^3, TR 4.2 s, acquisition time 2.1 s, interslice distance 0.5 mm, 20 slices.

2.3. Analysis

To identify the start of each MR scan period, a gradient method was employed: When the gradient of the signal between two data points exceeded 200 μV a marker has been set. All subsequent analyses were initially based on the same volume-start marker set. The feature of temporal drift detection of the Vision Analyzer V.1.05.0004 algorithm allows correction of the volume-start markers by the temporal drift between template and individual artifact. For this algorithm, corrected volume-start markers were used.

2.4. Determination of parameters

Since each algorithm offers the set-up of a number of parameters, we initially explored different combinations of parameters as listed in Table 1. This was done to determine reasonable parameters for the tested data sets. As a quality measure for artifact reduction, the ratio between the root mean square (rms) of uncorrected gradient-artifact EEG periods and corrected gradient-artifact periods was calculated. A strong reduction of the signal due to artifact elimination is necessarily accompanied by a high rms-ratio value. As a performance criterion, however, biosignal preservation is also relevant. Therefore, we also compared rms values of corrected nonartifact periods and original nonartifact periods to determine whether the biosignal was altered after artifact correction. A ratio of 1 indicates preservation of the original EEG data, whereas a deviation from 1 implies impairment of the physiological data by the correction algorithm. A ratio of 1 also could be obtained in situations when the spectral composition of the artifact-corrected signal is different from that of the original data but yields similar rms values. To exclude such scenarios, band-specific analyses were performed in a subsequent step.

Both sufficient artifact reduction and physiological signal preservation are necessary for a meaningful evaluation of artifact correction algorithms. Therefore, the combination of both criteria formed the basis for the selection of a reasonable parameter set.

2.5. Spectral band-specific evaluation of algorithm performance

After selection of the adequate parameter settings for each algorithm, band-specific algorithm performance was assessed. To this end, EEG data were segmented into

Table 1
Parameter sets of the three algorithms: a reasonable parameter set for each algorithm was determined by evaluating the performance of each algorithm with different parameter combinations ('evaluated parameters')

Algorithm	Constant parameters	Evaluated parameters	Selected parameters
ITAS	Epoch length: −50 to 4200 (entire scan and inter-scan period) Baseline correction: −50 to 0 ms Cross-correlation factor: 0.975	Interpolation factor: 1, 5, 10, 15 and 20 Sliding average with window sizes of 5, 10 and 15 epochs	Interpolation factor: 15 Sliding average with window size: 10
FASTR	Epoch length: entire scan and inter-scan period	Interpolation factor: 1, 5 ,10 and 15 Sliding average with window size: 5, 10 and 15 epochs Optimal Basis Set (OBS): on and off	Interpolation factor: 15 Sliding average with window size: 10
Vision Analyzer	Epoch length: −50 to 2040 ms (MR-acquisition period) Baseline correction: −50 to 0 ms Cross-correlation factor: 0.975	All artifact epochs The initial 5, 10 or 15 epochs and correlating subsequent epochs Sliding average with window size: 5, 10, 15 and 20 epochs	Initial 10 epochs and selected subsequent epochs

The 'constant parameters' were not changed during the analysis. The best performing and therefore finally selected parameters are listed under 'selected parameters'.

120 artifact epochs (starting at MR acquisition onset, length 1.6 s) and 120 artifact-free epochs (starting 0.4 s after MR acquisition offset, length 1.6 s). Fast Fourier transformation (FFT, 8000 points) was calculated for each baseline-corrected epoch, and, subsequently, the resulting spectra were averaged selectively for artifact and nonartifact periods. As a result, we obtained three averaged spectra per subject: one for the corrected MR acquisition periods, one for the corrected non-MR acquisition periods and another for the uncorrected non-MR acquisition periods. Finally, for each condition the grand average over all five subjects was determined. We analyzed the amplitude of six conventional spectral bands: theta (1–4 Hz), delta (4.5–7.5 Hz), alpha (8–12 Hz), beta (12.5–30 Hz), gamma (30.5–100 Hz), omega (100–250 Hz). Spectral content in artifact and nonartifact epochs was compared in three different ways as schematically depicted in Fig. 1A. First, ratios between spectral amplitudes of MR acquisition periods vs. non-MR acquisition periods of the corrected EEG data were calculated. This was done in order to identify systematic differences between both types of epochs after artifact correction. Second, ratios between spectral amplitudes of corrected MR acquisition periods and uncorrected non-MR acquisition periods were calculated to identify differences between artifact-corrected epochs and the original EEG. Third, ratios between spectral amplitudes of corrected non-MR acquisition periods and uncorrected non-MR acquisition periods were determined. This was done to evaluate biosignal preservation after artifact correction.

2.6. Surrogate data

As another test for biosignal preservation and to illustrate the effects of artifact correction on the original 'physiological' signal, we inserted surrogate 'biosignals' into one EEG data set. The artificial signal consisted of continuous sinus waves at 3, 5, 10, 20, 30 and 120 Hz with a constant amplitude of 100 μV. These signals were linearly added to the EEG data. All three algorithms were applied on the modified data, and, subsequently, spectrograms (spectral range, 2–200 Hz; frequency resolution 0.5 Hz/8192 points; temporal resolution 1.4 s; overlap 2048 points) were calculated and compared. Since the surrogate signals cause a dominant entry in the respective spectral bands, it can easily be seen if the correction algorithm disrupts these traces. The surrogate 'biosignals' were not phase locked to the scan onset of the MR device to facilitate its cancellation during template estimation and thus avoiding its removal by template subtraction.

3. Results

3.1. Determination of parameters

Fig. 3A–C shows the rms ratios averaged over all five subjects for different algorithms and parameter settings. The higher the ratio value, the more the gradient artifact was reduced after correction. As previously mentioned, artifact reduction, as well as physiological signal preservation, is an important feature of artifact-correction algorithms. In order to evaluate signal preservation, the ratio of the rms values between all uncorrected gradient artifact-free periods and all corrected gradient artifact-free periods was determined. Fig. 3D–F shows deviations from a ratio of 1. Zero deviation indicates no modification of the artifact-free biosignal after artifact correction. Higher values, in contrast, indicate distortion of the biosignal by the algorithm. The aim was not to determine optimal parameter settings in general — possibly a futile attempt since each data set might have its specific optimal parameters. Rather, it aims at finding reasonable parameters for the tested algorithms. These were to hold constant for all subsequent analyses. A detailed description of the results of the different parameter settings is given in Appendix A. A combination of the results of artifact reduction and physiological signal preservation was used for the selection of parameter settings. For Vision Analyzer software, best results were obtained in 'selected scan interval' modus with inclusion of the first 10 scan intervals and those epochs correlating higher than 0.975. In the case of FASTR and ITAS, artifact reduction and EEG preservation behaved in an opposed manner in respect to the window size (FASTR) and interpolation (FASTR and ITAS). Therefore, an interpolation factor of 15 and a window size of 10 were selected for both algorithms for subsequent analyses. Since OBS is an extra feature of FASTR mainly distinguishing it from ITAS, this function was used in further analyses. Thus, window size of 10 and interpolation factor of 15 (if applicable) turned out to be appropriate parameters for all algorithms and were used for all subsequent tests (Table 1, right column). These parameter values were also employed for the evaluation of the latest versions of Vision Analyzer and FASTR.

3.2. Spectral band-specific artifact reduction and EEG preservation

After artifact correction of all five data sets with each of the five algorithms (Analyzer 1.05.0002, Analyzer 1.05.0004, ITAS, FASTR 1.2b, FASTR 1.21) and with the previously specified parameters (Table 1 right column), we analyzed the amplitude of six spectral bands using FFT. In Fig. 1B, left column, spectral amplitudes of corrected MR acquisition periods (x-axes) and of corrected non-MR acquisition periods (y-axes) for all frequency bands, algorithms and subjects are depicted. The blue diagonal line marks an amplitude ratio (corrected nonacquisition period vs. corrected acquisition period) of 1, which indicates that the spectral amplitudes of MR acquisition epochs are equal to non-MR acquisition epochs after artifact correction. In the spectral range 1–30 Hz (delta to beta band), all three algorithms seem to correct the artifacts with similar quality (all results close to a ratio of 1). In the gamma and omega range (30.5–100 Hz), FASTR and ITAS yield ratios close to 1. For the older version of the Vision Analyzer, spectral amplitudes of the corrected MR acquisition periods are

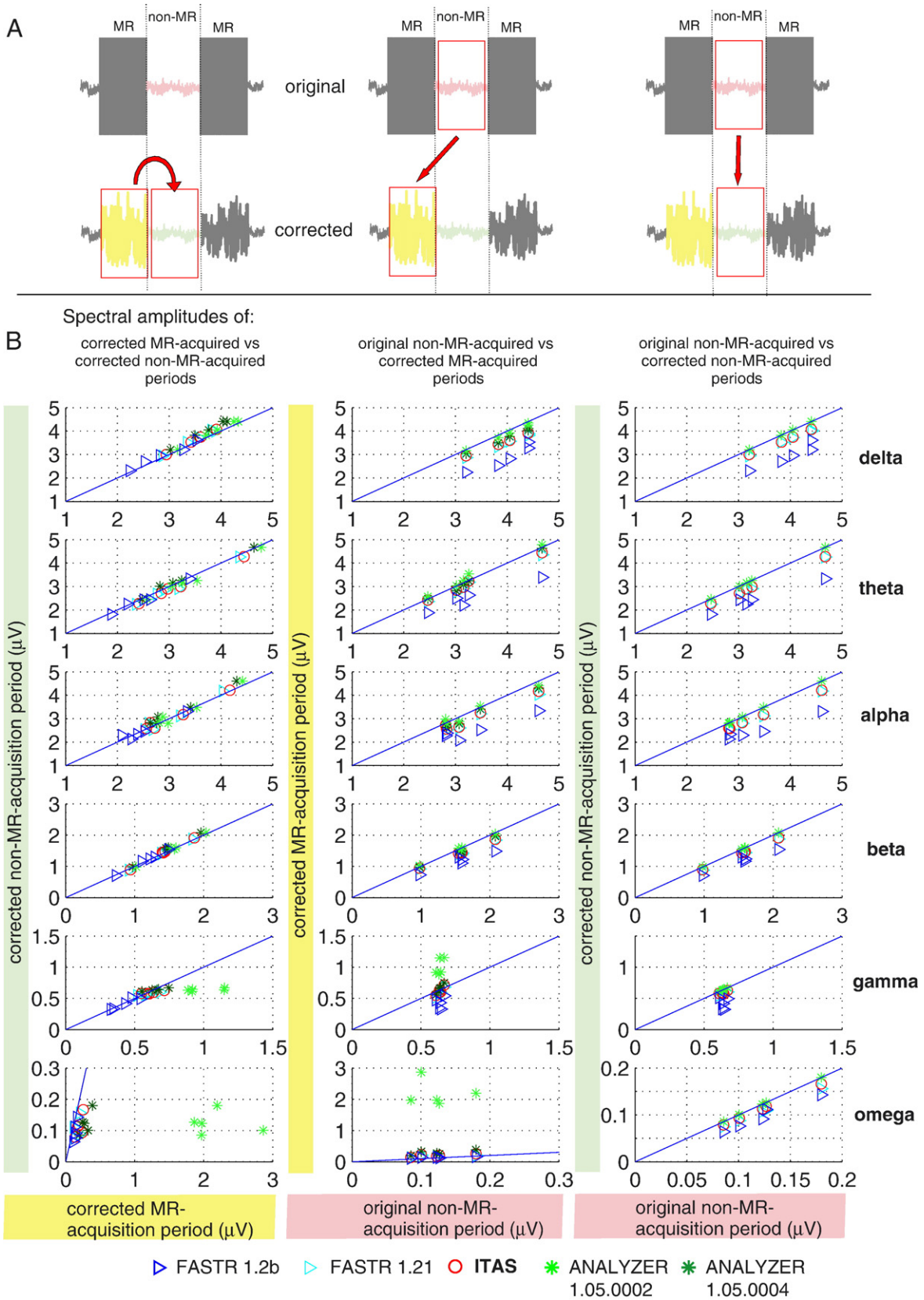

Fig. 1. Spectral band-specific artifact reduction and biosignal preservation. (A) Schematic illustration of the intervals that are compared in (B). (B) Column 1: Spectral amplitudes of corrected MR acquisition periods (x-axes) and corrected non-MR acquisition periods (y-axes). Column 2: Spectral amplitudes of original non-MR acquisition periods (x-axes) and corrected MR acquisition periods (y-axes). Column 3: Spectral amplitudes of original non-MR acquisition periods (x-axes) and corrected non-MR acquisition periods (y-axes). The blue diagonal line in each plot indicates a ratio of 1.

Table 2
Spectral band-specific ratios: between amplitudes of corrected MR-acquisition epochs and nonacquisition epochs (top), corrected MR-acquisition and uncorrected nonacquisition epochs (middle) and corrected nonacquisition and uncorrected nonacquisition epochs

	Algorithm	Delta	Theta	Alpha	Beta	Gamma	Omega
Corrected acquisition epochs vs. corrected nonacquisition epochs	ITAS	0.97	1.05	1.00	0.99	1.05	1.81
	Analyzer 1.05.0004	0.93	0.98	0.95	0.95	1.02	2.37
	FASTR 1.21	0.96	1.04	1.00	0.99	1.04	1.60
	Analyzer 1.05.0002	0.98	1.04	0.99	1.00	1.57	18.90
	FASTR 1.2b	0.97	1.03	1.01	0.99	1.02	1.46
Corrected acquisition epochs vs. uncorrected nonacquisition epochs	ITAS	0.90	0.96	0.91	0.91	0.97	1.62
	Analyzer 1.05.0004	0.93	0.98	0.95	0.95	1.02	2.31
	FASTR 1.21	0.88	0.94	0.90	0.90	0.93	1.29
	Analyzer 1.05.0002	0.98	1.04	0.99	1.00	1.56	17.20
	FASTR 1.2b	0.72	0.76	0.75	0.75	0.64	1.11
Corrected nonacquisition epochs vs. uncorrected nonacquisition epochs	ITAS	0.93	0.91	0.92	0.92	0.93	0.92
	Analyzer 1.05.0004	1.00	1.00	1.00	1.00	1.00	1.00
	FASTR 1.21	0.92	0.90	0.90	0.90	0.89	0.87
	Analyzer 1.05.0002	1.00	1.00	1.00	1.00	1.00	1.00
	FASTR 1.2b	0.74	0.74	0.75	0.76	0.63	0.78

considerably higher (gamma, omega) than those of the corrected non-MR acquisition periods due to remnant high-frequency artifacts. In the newer Vision Analyzer version, however, amplitude ratios approximate to 1 also for the higher frequency bands.

This analysis yields information on similarity of formerly artifact-afflicted and artifact-free epochs after artifact correction. In case of large remnant artifacts, spectral amplitudes would be higher for artifact epochs. This test alone is insufficient for quality assessment of artifact reduction since similarity of the signal in artifact-afflicted and artifact-free epochs after artifact reduction can be due to different mechanisms. Extreme scenarios would be (I) perfect artifact reduction, (II) almost complete deletion of the signal in both

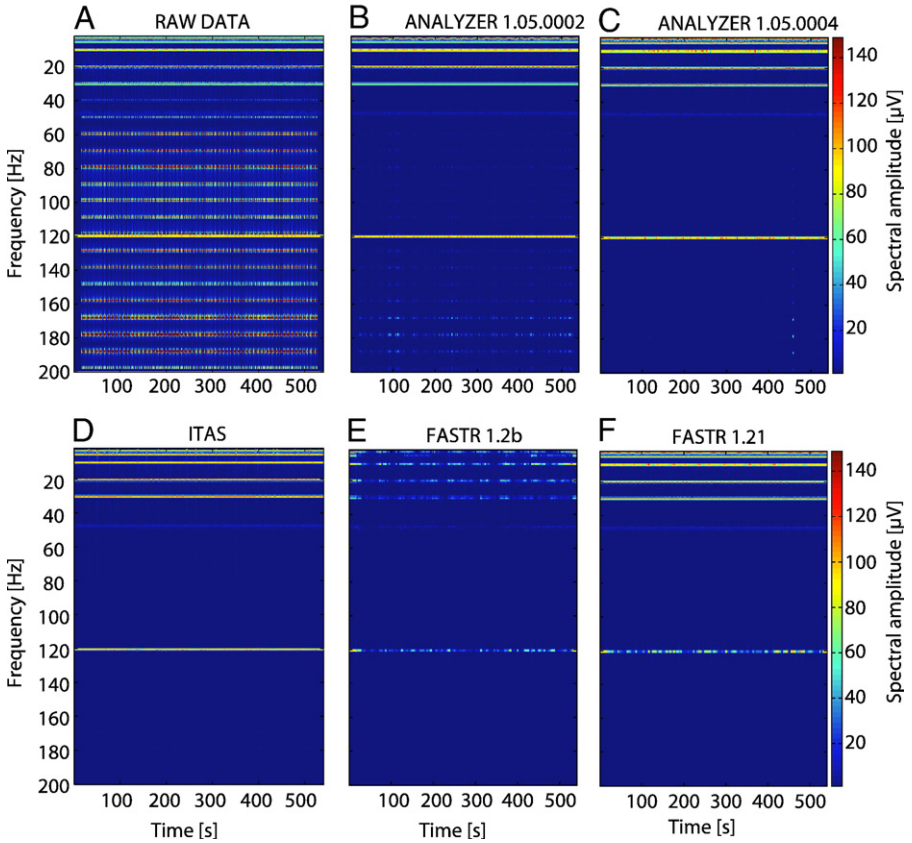

Fig. 2. Impact of artifact correction by different algorithms on surrogate signals. Top row, left: Spectrogram of surrogate data obtained by adding continuous artificial signals (sinus waves of 3, 5, 10, 20, 30 and 120 Hz frequencies; constant amplitudes of 100 µV) to the original EEG data. Surrogate data after artifact correction by the different algorithms are shown: Top row, middle: Analyzer software, version 1.05.0002. Top row, right: Analyzer software, version 1.05.0004. Bottom row, left: ITAS algorithm. Bottom row, middle: FASTR version 1.2b, bottom row, right: FASTR version 1.21.

epochs or (III) creation of a new signal that is equal in both types of epochs — but has nothing to do with the real EEG. To exclude the latter two cases, more tests are performed.

Therefore, in a second step, we compared the spectral amplitude of uncorrected artifact-free epochs and corrected artifact epochs (Fig. 1, middle column; Table 2). In lower spectral bands (delta to beta), all algorithms, with the exception of the old version of FASTR, yield similar satisfactory results. The older version of FASTR removes spectral content in all frequency bands for corrected acquisition epochs compared to uncorrected nonacquisition epochs. In the newer version of FASTR, in contrast, ratios are close to 1. In the gamma and omega range, the older Vision Analyzer version yields higher spectral amplitudes for corrected acquisition periods compared to the nonacquisition epochs. Again, the newer version approximates to a ratio of 1.

For the evaluation of biosignal preservation, we compared the spectral amplitudes of original vs. corrected nonacquisition epochs (Fig. 1, right column; Table 2). In contrast to the former comparison, which also provides partial information about biosignal preservation, algorithm-related modifications of identical EEG epochs are explored in this analysis. This yields additional valuable information, since systematic modifications of the physiological EEG signal across acquisition and nonacquisition epochs, e.g., due to differences in the acoustic noise or scanner vibrations, are precluded. Fig. 1B, right column, shows mean amplitudes of original non-MR acquisition periods (x-axes) and corrected non-MR acquisition periods (y-axes), the blue line again indicating a ratio of 1. Ratios below 1 indicate a reduction of the biosignal across artifact correction. In both versions of the Vision Analyzer software, artifact-free periods were not corrected and thus not modified. For the ITAS algorithm, only slight reductions of amplitudes can be seen. The older version of FASTR clearly reduces amplitudes of the EEG signal in non-MR acquisition periods in all spectral bands. The more recent version of FASTR performs similarly to the ITAS algorithm in terms of biosignal preservation.

In Table 2, all amplitude ratios of the analyses above are listed. In addition to Fig. 1, in Table 2 subtle performance differences between the algorithms are also discernible.

3.3. Surrogate data

In Fig. 2, the impact of artifact correction by different algorithms on surrogate signals is depicted. Fig. 2A shows the spectrogram of the sum of EEG plus surrogate data before artifact correction. The inserted surrogate signals at frequencies of 3, 5, 10, 20, 30 and 120 Hz as well as MR acquisition-related artifacts with their harmonics are clearly visible. Fig. 3B–F shows spectrograms of the artifact-corrected data. Vision Analyzer (Fig. 3B and C) preserves

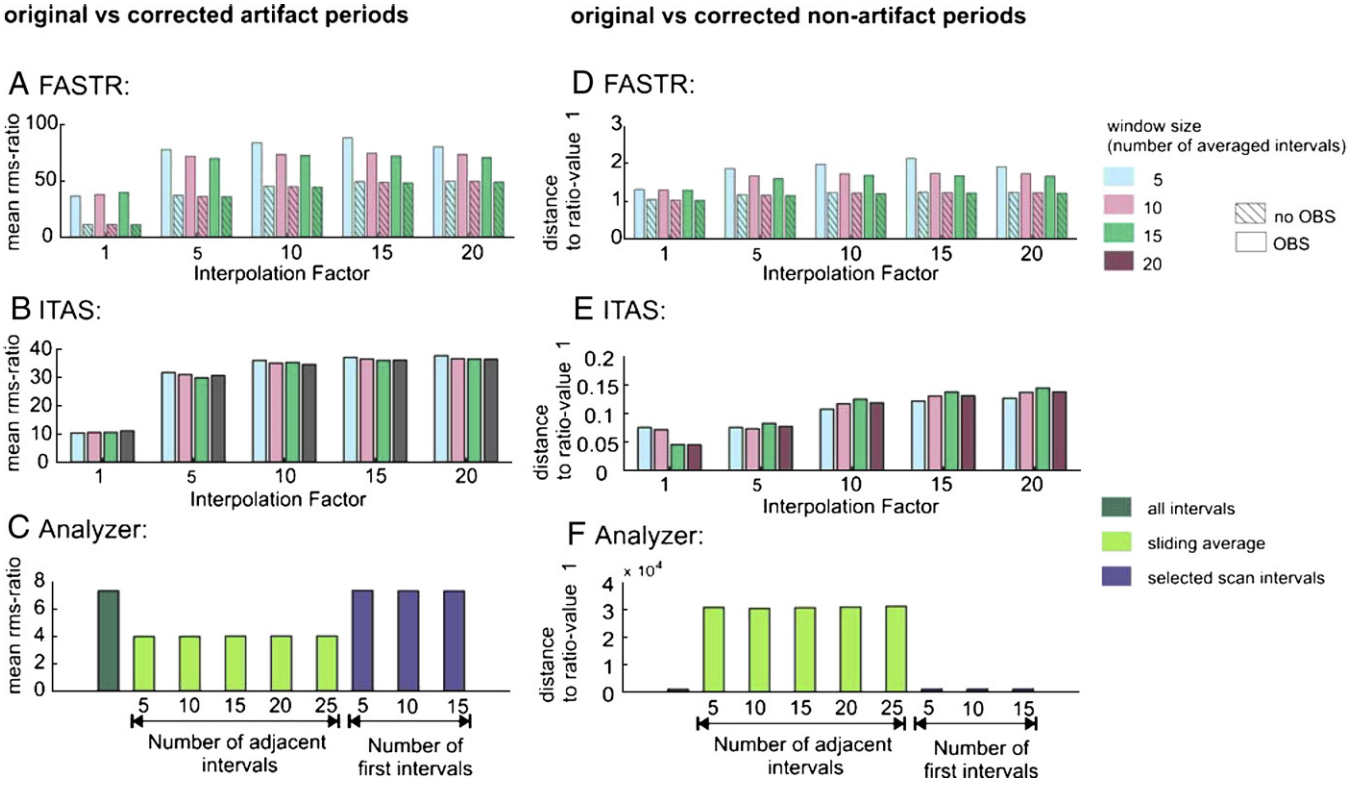

Fig. 3. Effects of parameter settings on artifact reduction for different algorithms. (A–C): For each parameter set, ratios between rms of uncorrected MR acquisition periods and corrected MR acquisition periods were calculated and averaged across all subjects. High ratios indicate strong signal reduction. (D–F): Average ratios between rms of uncorrected non-MR acquisition periods and corrected non-MR acquisition periods. The y-axis displays the absolute deviation from ratio 1, i.e., 0 indicates no difference between the nonacquisition EEG epoch before and after artifact correction.

the surrogate signals sufficiently. Remnant artifacts visible at higher frequencies when using the older Vision Analyzer version are considerably diminished by the newer version. ITAS (Fig. 2D) does not impair surrogate signals considerably and also show satisfying artifact reduction. The older version of FASTR (Fig. 2E) apparently impairs the surrogate signal. By using the updated version (Fig. 2F), surrogate signals are significantly less affected, with the exception of the surrogate signal at 120 Hz which still exhibits apparent amplitude reduction.

4. Discussion

In simultaneous continuous EEG–fMRI studies, the choice of an adequate artifact-removal algorithm has to be well considered. Since different algorithms are available, the issue of performance evaluation arises. With this study, we demonstrated that the amount of artifact reduction and the degree of physiological signal preservation are important complementary performance measures. Reduction of the artifact alone is not a quality measure since it provides no information on biosignal preservation. We have demonstrated that there are situations when a high degree of artifact reduction is paralleled by an undesired partial deletion of the biosignal. We also demonstrated performance differences in respect to different spectral bands. The beneficial effects of using the updated versions of both FASTR and Vision Analyzer with their respective feature extensions or improvements could be well documented in the present analysis. For example, in the updated FASTR algorithm the biosignal preservation was clearly improved (see Fig. 2E and F). Affliction of the original signal in the higher spectral range of 120 Hz can be attributed to the obligatory 70-Hz low-pass filter used when applying OBS. The updated Analyzer version and its TDD feature improved the removal of high-frequency components (see Fig. 2C and D). Staying up-to-date is apparently useful since algorithms are being improved continuously. We propose considering those performance differences when selecting a correction algorithm. Depending on the frequency spectrum of expected effects and the degree of averaging, the appropriate algorithm should be chosen. In this study, considerable differences have been demonstrated for algorithms all employing artifact template subtraction and also for different versions of the same algorithm. The results shown here are not meant to be generalized since results may differ for different experimental setups, conditions and individuals, and therefore performance measures should ideally be evaluated for each individual data set.

In this study, we have demonstrated an approach for the assessment of MR gradient artifact removal in a typical combined EEG–fMRI data set.

Acknowledgments

We would like to thank Peter Brunecker for helpful comments. This work was supported by the German Federal Ministry for Education and Research BMBF (Berlin Neuroimaging Center; Bernstein Center for Computational Neuroscience, Berlin).

Appendix A. Results: testing different parameter settings

A.1. Original vs. corrected artifact periods

FASTR: In order to evaluate the effect of OBS each combination of interpolation factor and window size has been run with and without OBS. Fig. 3A shows that higher interpolation results in a better reduction of the rms value up to an interpolation factor of 15. Also the window size (number of adjacent artifacts in the template calculation) has an apparent effect on artifact reduction. Using OBS results in better artifact reduction in all cases.

ITAS: Also for this algorithm interpolation factor and window size have been varied. Fig. 3B illustrates that interpolation results in a better artifact reduction. For higher interpolation, a higher ratio, i.e., more artifact reduction, is obtained up to an interpolation factor of 10. Higher interpolation factors do not significantly improve artifact reduction. Varying the window size has little effect. That highest ratios were achieved for lowest window size probably results from insufficient canceling out of the biosignal. Therefore, not only the artifact but also the biosignal is subtracted from the artifact-distorted EEG epoch.

Analyzer: We tested three different ways of calculating the average template for subsequent artifact correction. In Fig. 3C, it can be seen that using all artifact epochs or selected highly correlating intervals only for template calculation results in better artifact reduction than using the sliding average. Sliding average might perform better for longer acquisitions since the movement-related changes of artifacts over time become relevant. Varying the number of averaged intervals has only little effect on the results in the case of ‘sliding average’ calculation as well for ‘selected scan intervals’.

A.2. Original vs. corrected nonartifact periods

As previously mentioned, artifact reduction as well as physiological signal preservation is an important feature of correction algorithms. In order to evaluate signal preservation, the ratio of the rms values between all uncorrected gradient-artifact-free periods and all corrected gradient-artifact-free periods was determined. Fig. 3D–F shows deviations from a ratio of 1. No deviation indicates no modification of the artifact-free biosignal after artifact correction. Higher values in contrast indicate distortion of the biosignal by the algorithm.

FASTR: Fig. 3D shows that without OBS the EEG signal of gradient artifact-free periods is less modified by artifact correction. Variation of the interpolation factor or window size does not influence results significantly. On the other hand, using OBS shows a severe modification of the

'original' EEG signal. With the use of OBS, the window size affects the physiological signal preservation: a small window size results in stronger modification of the original EEG than choosing a larger window size.

ITAS: None of the parameter settings yields ratios deviating from the value of 1 with more than 0.15 indicating rms values of uncorrected artifact-free EEG epochs to be similar to those of the corrected artifact-free periods (Fig. 3E). The algorithm barely modifies the EEG signal. The higher the interpolation factor or number of window size, however, the more the EEG signal was modified.

Analyzer: Fig. 3F shows that the Analyzer algorithm does not remarkably influence the original EEG signal between MRI scans (effects are in the order of 10E-4).

References

[1] Ritter P, Villringer A. Simultaneous EEG–fMRI. Neurosci Biobehav Rev 2006;30(6):823–38.

[2] Feige B, Scheffler K, Esposito F, et al. Cortical and subcortical correlates of electroencephalographic alpha rhythm modulation. J Neurophysiol 2005;93(5):2864–72.

[3] Goldman RI, Stern JM, Engel Jr J, Cohen MS. Simultaneous EEG and fMRI of the alpha rhythm. Neuroreport 2002;13(18):2487–92.

[4] Goncalves SI, de Munck JC, Pouwels PJ, et al. Correlating the alpha rhythm to BOLD using simultaneous EEG/fMRI: inter-subject variability. Neuroimage 2006;30(1):203–13.

[5] Laufs H, Krakow K, Sterzer P, et al. Electroencephalographic signatures of attentional and cognitive default modes in spontaneous brain activity fluctuations at rest. Proc Natl Acad Sci U S A 2003;100(19):11053–8.

[6] Laufs H, Kleinschmidt A, Beyerle A, et al. EEG-correlated fMRI of human alpha activity. Neuroimage 2003;19(4):1463–76.

[7] Moosmann M, Ritter P, Krastel I, et al. Correlates of alpha rhythm in functional magnetic resonance imaging and near infrared spectroscopy. Neuroimage 2003;20:145–58.

[8] Bonmassar G, Anami K, Ives J, Belliveau JW. Visual evoked potential (VEP) measured by simultaneous 64-channel EEG and 3T fMRI. Neuroreport 1999;10(9):1893–7.

[9] Kruggel F, Wiggins CJ, Herrmann CS, von Cramon DY. Recording of the event-related potentials during functional MRI at 3.0 Tesla field strength. Magn Reson Med 2000;44(2):277–82.

[10] Liebenthal E, Ellingson ML, Spanaki MV, et al. Simultaneous ERP and fMRI of the auditory cortex in a passive oddball paradigm. Neuroimage 2003;19(4):1395–404.

[11] Czisch M, Wetter TC, Kaufmann C, et al. Altered processing of acoustic stimuli during sleep: reduced auditory activation and visual deactivation detected by a combined fMRI/EEG study. Neuroimage 2002;16(1):251–8.

[12] Czisch M, Wehrle R, Kaufmann C, et al. Functional MRI during sleep: BOLD signal decreases and their electrophysiological correlates. Eur J Neurosci 2004;20(2):566–74.

[13] Benar C, Aghakhani Y, Wang Y, et al. Quality of EEG in simultaneous EEG–fMRI for epilepsy. Clin Neurophysiol 2003;114(3):569–80.

[14] Iannetti GD, Di Bonaventura C, Pantano P, et al. fMRI/EEG in paroxysmal activity elicited by elimination of central vision and fixation. Neurology 2002;58(6):976–9.

[15] Krakow K, Lemieux L, Messina D, et al. Spatio-temporal imaging of focal interictal epileptiform activity using EEG-triggered functional MRI. Epileptic Disord 2001;3(2):67–74.

[16] Krakow K, Messina D, Lemieux L, et al. Functional MRI activation of individual interictal epileptiform spikes. Neuroimage 2001; 13(3):502–5.

[17] Lemieux L, Krakow K, Fish DR. Comparison of spike-triggered functional MRI BOLD activation and EEG dipole model localization. Neuroimage 2001;14(5):1097–104.

[18] Salek-Haddadi A, Merschhemke M, Lemieux L, Fish DR. Simultaneous EEG-correlated ictal fMRI. Neuroimage 2002;16(1):32–40.

[19] Salek-Haddadi A, Lemieux L, Merschhemke M, et al. Functional magnetic resonance imaging of human absence seizures. Ann Neurol 2003;53(5):663–7.

[20] Seeck M, Michel CM, Spinelli L, Lazeyras F. EEG mapping and functional MRI in presurgical epilepsy evaluation. Rev Neurol (Paris) 2001;157(8–9 Pt 1):747–51.

[21] Allen PJ, Polizzi G, Krakow K, et al. Identification of EEG events in the MR scanner: the problem of pulse artifact and a method for its subtraction. Neuroimage 1998;8(3):229–39.

[22] Bonmassar G, Purdon PL, Jaaskelainen IP, et al. Motion and ballistocardiogram artifact removal for interleaved recording of EEG and EPs during MRI. Neuroimage 2002;16(4):1127–41.

[23] Ives JR, Warach S, Schmitt F, et al. Monitoring the patient's EEG during echo planar MRI. Electroencephalogr Clin Neurophysiol 1993;87(6):417–20.

[24] Srivastava G, Crottaz-Herbette S, Lau KM, et al. ICA-based procedures for removing ballistocardiogram artifacts from EEG data acquired in the MRI scanner. Neuroimage 2005;24(1):50–60.

[25] Hoffmann A, Jager L, Werhahn KJ, et al. Electroencephalography during functional echo-planar imaging: detection of epileptic spikes using post-processing methods. Magn Reson Med 2000;44(5): 791–8.

[26] Sijbers J, Michiels I, Verhoye M, et al. Restoration of MR-induced artifacts in simultaneously recorded MR/EEG data. Magn Reson Imaging 1999;17(9):1383–91.

[27] Allen PJ, Josephs O, Turner R. A method for removing imaging artifact from continuous EEG recorded during functional MRI. Neuroimage 2000;12(2):230–9.

[28] Salek-Haddadi A, Friston KJ, Lemieux L, Fish DR. Studying spontaneous EEG activity with fMRI. Brain Res Brain Res Rev 2003;43(1):110–33.

[29] Becker R, Ritter P, Moosmann M, Villringer A. Visual evoked potentials recovered from fMRI scan periods. Hum Brain Mapp 2005;26(3):221–30.

[30] Schmid MC, Oeltermann A, Juchem C, et al. Simultaneous EEG and fMRI in the macaque monkey at 4.7 Tesla. Magn Reson Imaging 2006;24(4):335–42.

[31] Anami K, Mori T, Tanaka F, et al. Stepping stone sampling for retrieving artifact-free electroencephalogram during functional magnetic resonance imaging. Neuroimage 2003;19(2 Pt 1):281–95.

[32] Mandelkow H, Halder P, Boesiger P, Brandeis D. Synchronization facilitates removal of MRI artefacts from concurrent EEG recordings and increases usable bandwidth. Neuroimage 2006;32(3):1120–6.

[33] Delorme A, Makeig S. EEGLAB: an open source toolbox for analysis of single-trial EEG dynamics including independent component analysis. J Neurosci Methods 2004;134(1):9–21.

[34] Niazy RK, Beckmann CF, Iannetti GD, et al. Removal of FMRI environment artifacts from EEG data using optimal basis sets. NeuroImage 2005;28(3):720–37.

[35] Bandettini PA, Wong EC, Hinks RS, et al. Time course EPI of human brain function during task activation. Magn Reson Med 1992; 25(2):390–7.

[36] Frahm J, Bruhn H, Merboldt KD, Hanicke W. Dynamic MR imaging of human brain oxygenation during rest and photic stimulation. J Magn Reson Imaging 1992;2:501–5.

[37] Kwong KK, Belliveau JW, Chesler DA, et al. Dynamic magnetic resonance imaging of human brain activity during primary sensory stimulation. Proc Natl Acad Sci U S A 1992;89:5675–9.

[38] Ogawa S, Tank DW, Menon RS, et al. Intrinsic signal changes accompanying sensory stimulation: functional brain mapping with magnetic resonance imaging. Proc Natl Acad Sci U S A 1992; 89:5951–5.